Supporting information

Magnetic-Field-Induced Growth of Silver Dendrite-Crystalline Liesegang Rings

Qian Zhao, Jing Li, Shiyi Tang, Yongzhi Zhang, Li Chen, Martin M. F. Choi, Yong Guo,* Dan Xiao*

(Ⅰ) Experimental details

Chemicals: All of the materials required in our experiment are readily available: a zinc (Zn) plate (> 99%, Shanghai Xingta chemical plant, China) and a silver sulfate (Ag_2SO_4, Tianjin Kermel Chemical Reagents, China) aqueous solution, ultrapowerful Nd-Fe-B permanent magnetic alloy (50×50×25 mm, Shanghai Yongsheng magnetic industry, China). The magnetic induction intensity is measured by the Teslameter (WT10A, Henan Weite magnetic technology company, China).

Synthetic Method: In a typical experiment, the Zn plate (diameter 6 mm) was firstly polished with fine sand paper, until both of the two sides were smooth. Then the Zn plate was treated with dilute sulfuric acid, washed with triply distilled (TDI) water, and finally ultrasonicated in TDI water for 2 min to remove the surface debris and impurities. The pre-treated Zn plate was then immersed into a 5.5 cm diameter, 0.2 cm thick glass Petri dish containing 14 mL of 5.0 mmol L^{-1} Ag_2SO_4 aqueous solution. The magnetic field of the different orientations and sizes was applied in the system in order to observe the different growth states of Ag dendrites.

Characterization: The samples were characterized by SEM measurements, which were obtained with a Hitachi S4800 field emission scanning electron microscope

(Tokyo, Japan). Transmission electron microscopy (TEM), selected area electron diffraction (SAED), high-resolution transmission electron microscopy (HRTEM) images were acquired on a FEI Tecnai G^2 20 TEM (Hillsboro, OR, USA) operating at 200 kV. The crystal structure and phase purity of the prepared samples were analyzed using a Tongda TD-3500 X-ray powder diffractometer (Liaoning, China) with Cu Kα radiation (λ = 0.15418 nm) operating at 30.0 kV and 20.0 mA.

(Ⅱ) The details of the dynamics of ions in the system

We now propound the simplified reaction schemes, followed by the reaction-diffusion equations describing the dynamics, now augmented by the magnetic field interaction term for the charged species.

We introduce the following variables:

$$X = Ag^{+}(\mathrm{aq})$$
$$\mathrm{Y} = \mathrm{Zn(s)}$$
$$Z = Zn^{2+}(\mathrm{aq})$$
$$\mathrm{A} = \mathrm{Ag(s)}$$

The Ag-Zn galvanic displacement reaction scheme is reduced to a simpler form as follows:

$$2X + Y \xrightarrow{k} Z + 2A \tag{1}$$

The conservation equations for the concentrations of the various species diffusion and reacting are given by

$$\partial X(\mathrm{x,t}) / \partial \mathrm{t} = \mathrm{D}_x \, \partial^2 X / \partial \xi^2 - 2kX^2 Y \tag{2}$$

$$Y(\mathrm{x,t}) \equiv 0 \tag{3}$$

where D_X is diffusion coefficient of X; ξ is a 2D spatial variable; k is a reaction rate constant. In our system, the Ag^+ and Zn are reacting irreversibly. The magnetic

field does not affect the extent of the reaction.

It is reasonable to conclude that the primary effect of the magnetic field is to promote the ions transfer rate. The increase of mass transfer in the field must be due to some forces possibly giving rise to the observed effects.

The Lorentz force $\vec{F}_L$ acts on moving ions in a magnetic field and appears when magnetic field lines cross the electric field lines:

$$\vec{F}_L = \vec{j}(\mathrm{t}) \times \vec{B} \tag{4}$$

where $\vec{j}(\mathrm{t})$ is the local flux of ions and $\vec{B}$ is the magnetic flux density. $\vec{F}_L$ acts in the hydrodynamic layer and is accepted as the main driving force of the so-called magnetohydrodynamic (MHD) effect, which is an increased convection in the magnetic field.

As we known, there is a diffusion layer immediately adjacent to the surface of the Zn plate where the concentration of Ag^+ changes rapidly from zero to its value in the bulk solution when it is immersed in the Ag_2SO_4 solution. The concentration difference between the diffusion layer and the bulk solution normally drives convection, the direction of which is from the Ag ion-rich solution to the Ag ion-depleted solution. It is believed that the force due to a concentration gradient drives Ag^+ toward the surface of the Zn plate, where the very rapid galvanic displacement reaction occurs as a result of the electrical potential difference between the Ag^+/Ag and the Zn^{2+}/Zn pairs. What we call the force is the concentration gradient force, denoted as $\vec{F}_C$. The driving force for diffusion is:

$$\vec{F}_C = RT\vec{\nabla}C \tag{5}$$

$\vec{\nabla}C = C_h - C_l$. C_h is the high concentration of the ions and C_l is the low concentration of the ions.

And the gravity force $\vec{F}_G$ is:

$$\vec{F}_G = m\vec{g} \tag{6}$$

When LR is grown in the nonuniform magnetic field, the field gradient force exists:

$$\vec{F}_B = \chi_m CB\vec{\nabla}B / \mu_0 \tag{7}$$

Where χ_m is the molar susceptibility of Ag^+, μ_0 is the permeability of a free space.

The Navier-stokes equation expresses the Newton's second law for an incompressible fluid element.

$$\partial\vec{v} / \partial t + \vec{v}\nabla\vec{v} = -\vec{\nabla}P / \rho + \upsilon\nabla^2\vec{v} + \vec{F}_i \tag{8}$$

The left-hand side of the equation is the acceleration of the fluid element. The first term on the right-hand side is the pressure gradient force and the second term is the viscous force, which could be negligible through our system. The third term, $\vec{F}_i$, refers to any other external volume forces including the four forces mentioned above. Therefore, the velocity profile of Ag^+ in the solution can be derived from Eqs. (4)-(8).

$$\partial\vec{v} / \partial t + \vec{v}\nabla\vec{v} = \vec{j}(\mathrm{t}) \times \vec{B} + RT\vec{\nabla}C + m\vec{g} + \chi_m CB\vec{\nabla}B / \mu_0 \tag{9}$$

(III) Supporting figures and tables

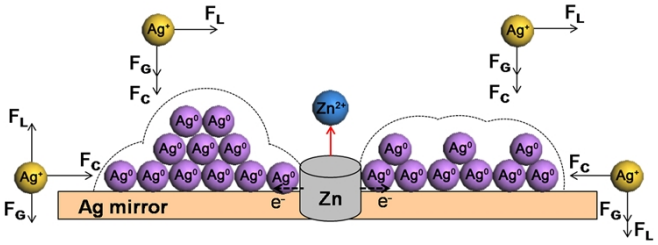

FIG. S1 Schematic presentation of nucleation and growth phenomena with superimposed magnetic field in parallel upward to the glass Petri dish.

While applying the upward parallel magnetic field in the system [Fig. 1(d)], the Ag^+ in the upper solution could obtain a maximum $\vec{F}_L$. The rings had a trend of the

rightward motion in the mass. In the red rectangle, the Ag NPs were more aggregated and closer to the Zn plate, while the ones in the blue rectangle stretched rightwards away from the plate. In addition, the Ag^+ at the bottom also had a $\vec{F}_L$, which promoted the formation of the asymmetrical oval LR (Fig. S1). The Ag^+ in the green rectangle and the yellow rectangle were less influenced.

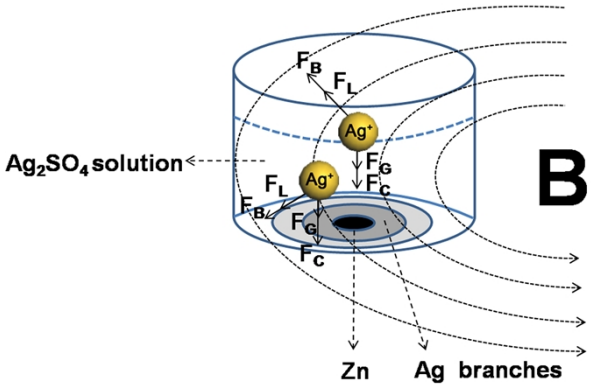

FIG. S2 Schematic presentation of nucleation and growth phenomena with superimposed nonuniform magnetic field.

We take Fig. 4(h) as an example to illustrate the formation mechanism of the LRs in the nonuniform magnetic field (Fig. S2). The inner Ag^+ had an inward $\vec{F}_L$ while the outer Ag^+ had an outward $\vec{F}_L$. Moreover, the direction of the field gradient force ($\vec{F}_B$) was basically same to the one of $\vec{F}_L$ due to the maximum field gradient. Then an obvious gap occurred in the left of the LR.

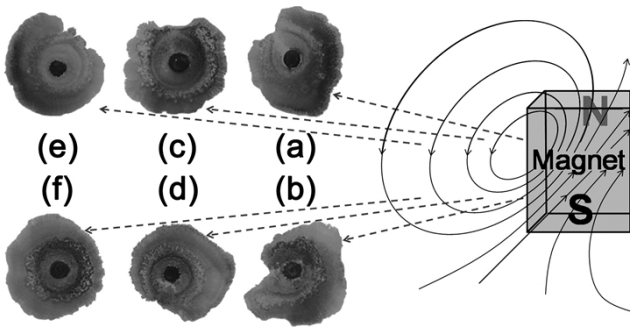

FIG. S3 The photographs of LRs in nonuniform in-plane magnetic field: (a) and (b) 20 mT; (c) and (d) 5 mT; (e) and (f) 2 mT.

In order to further observe the influence of magnetic field with different magnetic induction strength on LRs, the following experiments were made. The glass Petri dishes were placed near and far in two positions corresponding to the Fig. 4(g) and 4(i). The LRs were less influenced if the samples were kept away from the magnet [Fig. S3(e) and S3(f)]. It was also found that the opening directions of gaps were corresponding to the directions of magnetic field.

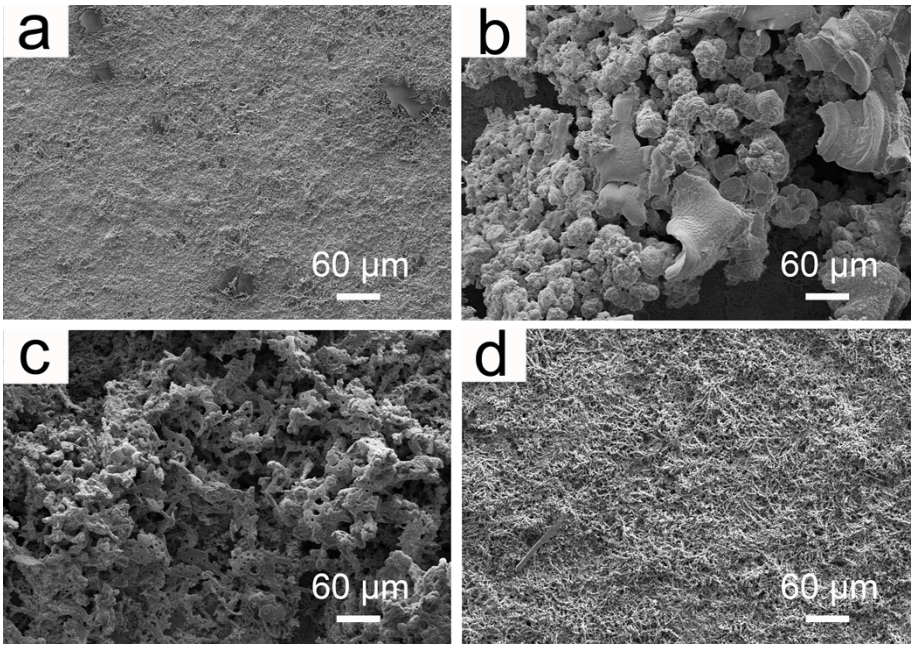

FIG. S4 Lower SEM images of LRs at about 45 min in uniform magnetic field: (a) 0 T; (b) 0.4 T vertically upward; (c) 0.4 T vertically downward; (d) 0.4 T horizontally upward.

The Figure S4 shows the lower SEM images of LRs corresponding to Figure 1. The surface of rings with imposed magnetic field is considerably rougher than the one without magnetic field, especially in vertical magnetic field (Figure S4b and S4c). The stems and branches of dendrite crystals could be seen in the Figure S4a and S4d. The structure of rings in vertical magnetic field is similar to amorphous crystals. The

thickness of them is increased and the distribution of them is nonuniform.

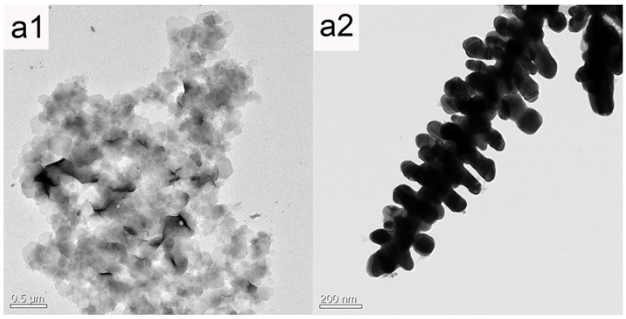

FIG. S5 TEM (a1) images of the inner part; TEM (a2) images of the outer part.

Fig. S5(a2) displays the Ag dendrites in the outer part. And Fig. S5(a1) shows the metallic Ag takes on thin flake-like shape, and too many of them interconnect with each other.

Table 2 Ratio of distances from the Zn plate of the rings in different parts (right, middle and left part) corresponding to Fig. 2(d).

Distance (mm) / Ring number	r_r	r_m	r_l	r_r/r_m	r_r/r_l
1	5.0	4.0	1.8	1.25	2.77
2	7.2	6.0	4.9	1.2	1.47
3	11.5	10.1	8.1	1.14	1.42

Table 3 Ratio of distances from the Zn plate of the rings in different parts corresponding to Fig. 3(i).

Distance (mm) / Ring number	r_A	r_B	r_C	r_D	r_A/r_B	r_A/r_C	r_A/r_D
1	2.0	2.0	6.2	2.0	1.0	0.32	1.0
2	2.8	5.8	9.3	3.5	0.48	0.30	0.8

3	3.9	10.4	-	6.4	0.375	-	0.61

From Table 2, it is shown that the rings extend towards the right. The larger ratios of right rings to left rings indicate the left side is an aggregated form. And it is clear from Table 3 that the rings extend towards the bottom left side, especially in Fig. 3(i)-C. It is the origin of the appearance of gap.

(Ⅳ) Application of the materials

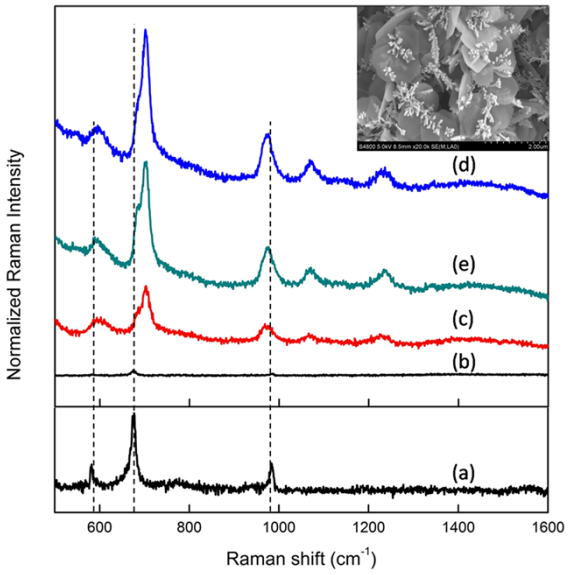

FIG. S6 Raman spectra of (a) solid melamine, (b) melamine on a blank Petri dish, (c) melamine adsorbed on inner LR, (d) melamine adsorbed on middle LR, and (e) melamine adsorbed on outer LR. Measurement was conducted from 500 to 1600 cm^{-1} with 4 s exposure time and 25 mW laser power. And the top right inset shows the SEM images of the middle transition zone corresponding to the Fig. S5d.

Typical Raman peaks of solid melamine at 583, 676, and 984 cm^{-1} are identified from Fig. S5a. The most intense peak at 676 cm^{-1} is assigned to the ring-breathing II mode, involving the in-plane deformation of the triazine ring. Another strong peak at 984 cm^{-1} arises from the ring-breathing mode I of the triazine ring.[1] No obvious peaks are obtained in Raman spectrum of the blank Petri dish [Fig. S5(b)]. For comparison,

stronger Raman signals can be observed using Ag NPs as the SERS substrate. It was also found that the Raman signals obtained from the outer LR of Ag dendrites [Fig. S5(e)] are much stronger than that of the inner LR of Ag NPs [Fig. S5(c)]. The signals obtained from the middle LR of Ag NPs [Fig. S5(d)], the transition zone of the Ag NPs of plate-like structure and the Ag dendrites, are strongest, the reason of which is that the Ag plates (the inset of Fig. S5) have thinner thickness and smaller sizes, which are flatter and sparser than the plate-like structure in the inner LR. A small quantity of Ag dendrites, sparser than those in the outer LR (Fig. 5), exists among these Ag plates. It is the sparser and smaller plate-like structure that can make maximum enhancement of the Raman signal of melamine.

The melamine peak at 699 is shifted by 25 cm^{-1}, which is a large shift compared to that of the solid melamine, due to chemical or electronic enhancement and the electromagnetic field effect of Ag NPs and Ag dendrites on the triazine ring of melamine.[2] It is clear that the relative intensities of the typical Raman peaks at 583, 676 and 984 cm^{-1} are much enhanced, and some unobvious and weaker Raman peaks of solid melamine at 1070 and 1230 cm^{-1} are also enhanced obviously and observed in Fig. S5(c), (d), (e). Here, the as-synthesized Ag NPs of plate-like structure, transformed from Ag dendrites via magnetic field, indeed enhance the Raman signal of melamine, providing a useful approach to the determination of melamine qualitatively.

Reference

[1] E. Koglin, B. J. Kip and R. J. Meier, J. Phys. Chem. 1996, **100**, 5078.
[2] X.-F. Zhang, M.-Q. Zou, X.-H. Qi, F. Liu, X.-H. Zhu and B.-H. Zhao, J. Raman Spectrosc. 2010, **41**, 1655.